ACS APPLIED NANO MATERIALS

www.acsanm.org

Article

First-Principles Investigation of Metallic Zr_2Se_2C Nanosheets with High Potential for Li-Ion Battery Anodes

Nicolas F. Martins,* Fredy Mamani Gonzalo, José A. S. Laranjeira, Victor J. R. Rivera, Pablo A. Denis, and Julio R. Sambrano*

Cite This: *ACS Appl. Nano Mater.* 2025, 8, 20792−20800

Read Online

ACCESS | Metrics & More | Article Recommendations | Supporting Information

ABSTRACT: Efficient energy sources are essential to meet the growing demand from households, electric vehicles, and portable devices. Thus, electrode materials with high capacity and safety are critical for battery advancement. Recently, metallic two-dimensional (2D) transition metal carbo-chalcogenides (TMCCs), such as Nb_2X_2C and Ta_2X_2C (X = S, Se), have shown promise for energy storage. In this context, we propose 2D Zr_2Se_2C as a novel Li-ion anode using first-principles calculations. This material exhibits favorable Li kinetics, with a low diffusion barrier of 0.20 eV. A single Li atom donates 0.23 *e* to the substrate, indicating an efficient charge/discharge rate. Moreover, Zr_2Se_2C can accommodate up to three Li layers on a double-sided scheme, yielding a high theoretical capacity of 456 mAh/g. An average open-circuit voltage of 0.53 V further supports its potential as an efficient TMCC-based anode.

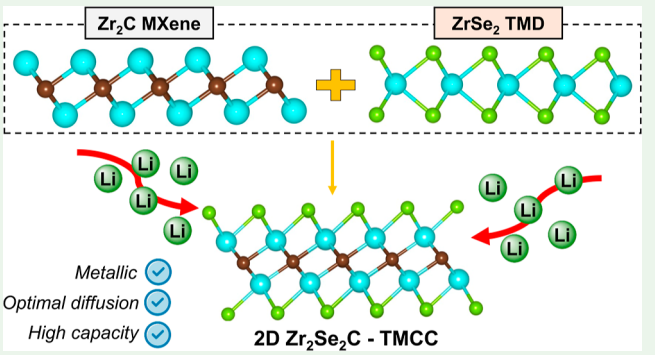

KEYWORDS: *MXene, LIBs, 2D materials, TMCC, DFT*

INTRODUCTION

Since the first commercialization of lithium-ion batteries (LIBs) in 1991, their market has expanded rapidly due to their high energy density and the relative abundance of lithium.[1,2] For example, the $LiCoO_2$/graphite system, representing the cathode and anode materials respectively, offered a specific energy of 100 Wh/kg in 1991. This value has since been significantly improved through continuous research, reaching approximately 280 Wh/kg by 2020.[3] The growing demand for energy, driven by the proliferation of portable electronic devices and electric vehicles, has fueled a global pursuit of more efficient rechargeable batteries, including LIBs.[4,5] Graphite, the most widely used anode material, offers a storage capacity of only 372 mAh/g,[6] which limits its applicability in large-scale energy storage systems. Consequently, considerable efforts have been directed toward discovering alternative electrode materials with superior conductivity, enhanced Li-ion diffusion, and favorable electrochemical kinetics.

In this context, two-dimensional (2D) materials have emerged as promising candidates for next-generation energy storage technologies. Their inherently high surface-to-volume ratio, low dimensionality, and advantageous ion migration channels offer key benefits.[7−9] Additionally, quantum confinement effects in 2D materials often result in intrinsic metallicity, a critical factor for ensuring both battery safety and cycling stability. Among these, transition metal dichalcogenides (TMDs) have shown great potential in energy storage applications, particularly in LIBs. Notable examples include MoS_2,[10] WS_2,[11] $MoSe_2$,[12] and WSe_2.[13] Similarly, MXene-based structures—discovered in 2011—have attracted substantial attention for their robust mechanical stability and high electrical conductivity.[14−19]

More recently, a new class of 2D materials has been introduced by integrating the properties of both TMDs and MXenes, resulting in the so-called 2D transition metal carbo-chalcogenides (TMCCs). These nanostructures exhibit a MXene-like carbide skeleton, typically terminated by chalcogen atoms such as sulfur or selenium. The first successful synthesis of such a material was Nb_2Se_2C, in which Nb motifs from the TMD-like $NbSe_2$ were replaced with Nb−C layers from a MXene-like Nb_2C matrix.[20] In 2022, Majed et al.[21] reported the synthesis of sulfur-based TMCCs, including Ta_2S_2C and Nb_2S_2C, via a novel approach involving lithium intercalation and delamination of their bulk precursors. Electrochemical evaluations revealed excellent anode performance for Nb_2S_2C, in agreement with earlier density functional theory (DFT)

Received: July 17, 2025
Revised: October 10, 2025
Accepted: October 13, 2025
Published: October 20, 2025

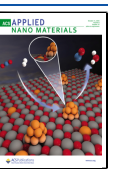

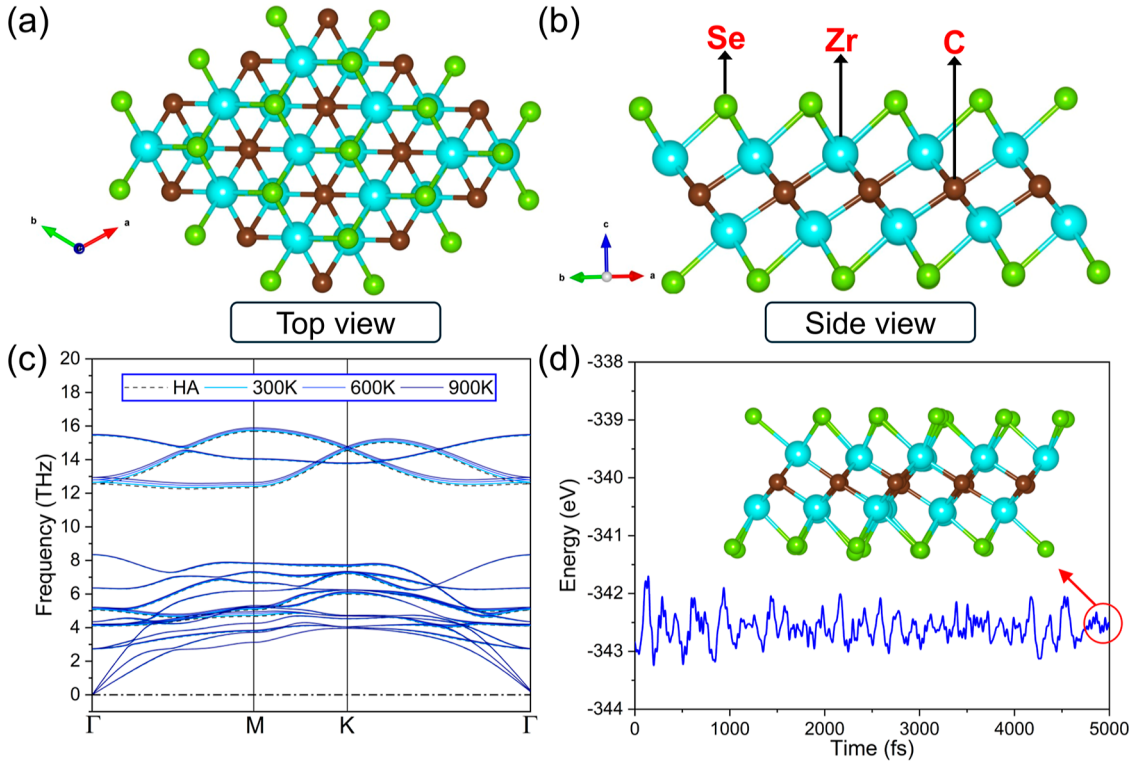

Figure 1. (a) Top and (b) side perspectives of Zr_2Se_2C monolayer. (c) Temperature-dependent phonon dispersion and (d) ab-initio molecular dynamics (AIMD) at 300 K for 2D Zr_2Se_2C.

predictions by Jing et al.,[22] who reported high metallicity and metal storage capacities ranging from 158 to 691 mAh/g. Building on these breakthroughs, Loni et al.[23] expanded the TMCC family by synthesizing Ta_2Se_2C through electrochemical lithiation, demonstrating both theoretically and experimentally its promising catalytic activity for the hydrogen evolution reaction (HER). Recently, Martins et al.[24] explored computationally 2D Ta_2Se_2C as an anode material for Li and Na-ion electrodes, achieving optimal theoretical capacity and high diffusion kinetics. Sun and colleagues[25] also demonstrated that different transition metal carbo-sulfides can be alternative substrates for lithium−sulfur (Li−S) batteries. Numerous theoretical studies have since supported these experimental findings or proposed new applications for TMCCs in energy storage, gas sensing, and conversion.[26−30]

Motivated by recent advances, we explore the Zr_2Se_2C monolayer as a novel TMCC-based anode material for Li-ion batteries through comprehensive DFT simulations. We evaluate its structural, electronic, and mechanical properties, along with the lithium storage capacity and diffusion behavior on this new 2D material. Our results demonstrate that 2D Zr_2Se_2C possesses excellent anodic performance, representing a promising direction for the development of next-generation 2D TMCC materials in energy storage applications.

COMPUTATIONAL SETUP

First-principles calculations based on density functional theory (DFT) were conducted using the Vienna ab initio simulation package (VASP).[31] The projector augmented wave (PAW) method and the Perdew−Burke−Ernzerhof (PBE) functional within the generalized gradient approximation (GGA) were utilized.[32,33] A plane-wave energy cutoff of 520 eV was applied to guarantee convergence accuracy. For the relaxation of atomic structures, a Monkhorst−Pack *K*-point mesh of 6 × 6 × 1 was employed, whereas the electronic density of states (DOS) was calculated using a denser Γ-centered mesh of 12 × 12 × 1. To incorporate van der Waals interactions, the DFT-D3 correction proposed by Grimme was implemented.[34] Structural optimizations were performed using the conjugate gradient method until predefined convergence thresholds were satisfied. Total energy differences were limited to below 1×10^{-5} eV, and atomic forces were reduced to less than 0.01 eV/Å. A vacuum spacing of 20 Å was introduced along the *z*-direction to suppress spurious interactions between periodic slabs.

To evaluate the dynamical stability of the 2D Zr_2Se_2C monolayer, phonon dispersion calculations were performed using ALAMODE[35,36] with 3 × 3 × 1 supercell. Additionally, ab initio molecular dynamics (AIMD) simulations were conducted at 300 K for 5 ps in the *NVT* ensemble, employing the Nosé−Hoover thermostat[37] to assess its thermal robustness. For the lithiated system, a simulation time of 10 ps was considered. A 3 × 3 × 1 supercell containing a single adsorbed metal atom was employed to investigate the adsorption and diffusion behavior of metal ions on Zr_2Se_2C. The diffusion energy barriers and minimum energy paths were determined using the climbing image nudged elastic band (CI-NEB) method. In these calculations, the force convergence criterion was set to be below 1×10^{-3} Ry/a.u.

RESULTS AND DISCUSSION

Structural and Electronic Description. The two-dimensional Zr_2Se_2C monolayer originates from the hybridization of $ZrSe_2$ and Zr_2C, which correspond to prototypical TMD and MXene-like structures, respectively. This shape results in the retention of the carbon-rich core from the MXene precursor,

https://doi.org/10.1021/acsanm.5c03369
ACS Appl. Nano Mater. 2025, 8, 20792−20800

along with alternating zirconium and selenium atoms arranged in a layered configuration, as illustrated in Figure 1a,b from top and side views. The Zr_2Se_2C TMCC adopts a hexagonal crystal structure with optimized lattice constants of $a = b = 3.45$ Å, exceeding the experimental values reported for 2D Ta_2Se_2C (3.31 Å)[23] and 2D Nb_2Se_2C (3.32 Å).[20] The theoretical lattice constant of 2D Zr_2Se_2C is compared with other 2D TMCCs (Ta_2Se_2C, Nb_2Se_2C, Ta_2S_2C, and Nb_2S_2C), as listed in Table S1. In addition, we estimated the formation energy of 2D Zr_2Se_2C to be −2.57 eV, which is lower (less stable) than those of the Ta- and Nb-based analogues (−2.75 and −3.24 eV, respectively).

The mechanical response of 2D Zr_2Se_2C was investigated and compared with its TMCC analogues. As the crystal exhibits hexagonal symmetry, the number of independent elastic constants can be reduced to C_{11} and C_{12}, while the shear constant (C_{66}) can be obtained from $(C_{11} - C_{12})/2$. Accordingly, the stiffness matrix of these 2D TMCC materials can be expressed as

$$C_{ij} = \begin{pmatrix} C_{11} & C_{12} & 0 \\ C_{12} & C_{11} & 0 \\ 0 & 0 & C_{66} = (C_{11} - C_{12})/2 \end{pmatrix} \quad (1)$$

The elastic constants of 2D Zr_2Se_2C were found to be C_{11} = 244.23 N/m, C_{12} = 55.23 N/m, and C_{66} = 90.05 N/m. These values, along with those calculated for other 2D TMCCs, are reported in Table S1. All of these structures satisfy the Born−Huang criteria for mechanical stability in 2D hexagonal lattices, namely $C_{11} > 0$, $C_{66} > 0$, and $C_{11}C_{22} - C_{12}^2 > 0$.[38] Furthermore, it can be observed that Se-terminated surfaces exhibit slightly higher rigidity compared to their S-based counterparts.

When predicting novel 2D materials via DFT, it is essential to assess both their dynamic and thermal stabilities. Phonon dispersion analysis is commonly employed to verify dynamic stability by checking for the absence of imaginary modes, while ab initio molecular dynamics (AIMD) simulations are used to evaluate thermal stability under finite-temperature conditions. As shown in Figure 1c, the phonon spectrum exhibits no imaginary frequencies across the high-symmetry paths of the Brillouin zone, both in vacuum and at various temperatures ranging from 300 to 900 K, confirming the dynamical stability of the monolayer. Furthermore, AIMD simulations conducted at room temperature demonstrate that the Zr_2Se_2C structure maintains its geometric integrity throughout the simulation, as evidenced by the final snapshot depicted in Figure 1d.

The electronic properties of the 2D Zr_2Se_2C material are presented in Figure 2. The electronic band structure confirms its metallic character, as evidenced by several crossing the Fermi level (set to zero). This metallic behavior is particularly advantageous for potential anodic applications. Notably, the metallicity of 2D Zr_2Se_2C can be attributed to the significant overlap between Zr d- and p-states of Se and C atoms, as illustrated in the projected density of states (PDOS) plot.

Li Binding and Diffusion on Zr_2Se_2C Monolayer. To comprehensively evaluate the potential of the Zr_2Se_2C TMCC monolayer as a Li-ion battery anode, it is essential to investigate its lithium storage mechanism. For this purpose, a 3 × 3 × 1 supercell of the monolayer is constructed, and a single Li atom is systematically placed above various high-symmetry adsorption sites. These sites correspond to the top of the surface atoms, namely Se, Zr, and C, as illustrated in Figure 1. The adsorption energy (E_{ads}) is calculated using the following expression

$$E_{ads} = E_{Zr_2Se_2C+Li} - E_{Zr_2Se_2C} - E_{Li} \quad (2)$$

where $E_{Z_2Se_2C+Li}$ denotes the total energy of the Li-adsorbed system, $E_{Zr_2Se_2C}$ is the energy of the pristine monolayer, and E_{Li} corresponds to the energy of an isolated Li atom in vacuum. A more negative E_{ads} value implies a more thermodynamically favorable (i.e., more stable) adsorption site. The corresponding adsorption energies are summarized in Figure 3a. Among the evaluated sites, the Zr site exhibits the most favorable interaction, with an E_{ads} of −2.93 eV. This value indicates a significantly stronger binding affinity compared to several reported TMCC and MXene systems, such as Zr_2C (−2.23 eV),[39] Nb_2S_2C (−1.67 eV),[22] and $Zr_3C_2S_2$ (−2.20 eV).[40]

The fully relaxed geometry of the Li-adsorbed Zr_2Se_2C system is presented in Figure 3b. To further explore the electronic interaction between Li and the TMCC substrate, Bader charge analysis was performed. The results reveal a charge transfer of approximately 0.23 e from the Li atom to the monolayer, indicating effective charge donation. When a substantial charge is transferred from the metal to the host substrate, as observed for Li on 2D Zr_2Se_2C, the result is an increase in electrical conductivity and a more stable lithiation

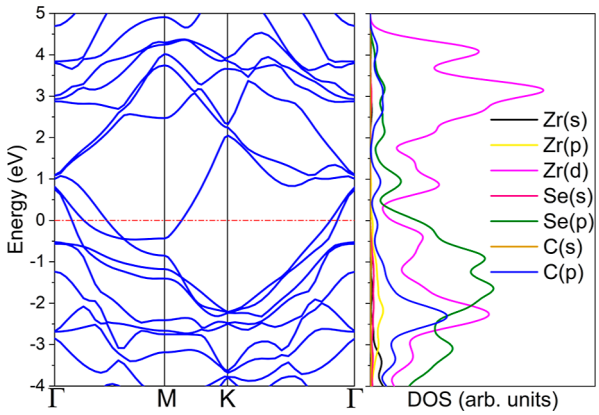

Figure 2. Band structure and projected density of states (PDOS) of 2D Zr_2Se_2C.

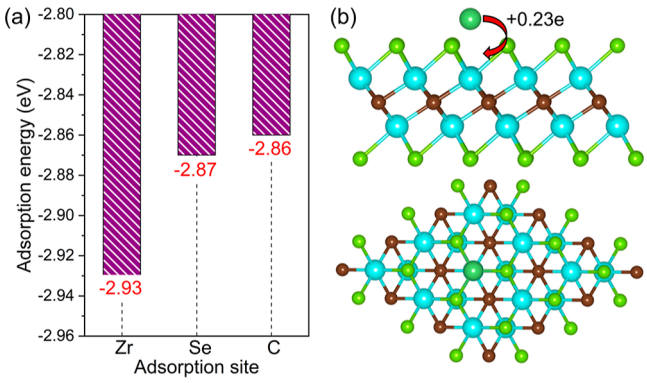

Figure 3. (a) Computed adsorption energies for Li over each available site on 2D Zr_2Se_2C (Zr, Se, and C). (b) Side and top views of the most stable configuration (above Zr site) with the register of Bader charge result.

https://doi.org/10.1021/acsanm.5c03369
ACS Appl. Nano Mater. 2025, 8, 20792−20800

process, since the metal is more effectively retained on the surface due to strong binding interactions.

Understanding metal-ion mobility across the electrode surface is crucial for evaluating the practical feasibility of battery systems. In this context, Li diffusion behavior on the 2D Zr_2Se_2C monolayer was investigated using the CI-NEB method. As illustrated in Figure 4a, three distinct migration pathways were identified for Li diffusion on the substrate, denoted as Paths 1, 2, and 3. Path 1 corresponds to the direct migration of a Li atom between adjacent Zr top sites. In contrast, Path 2 represents diffusion along the Se centers, while Path 3 traces the migration across the carbon sites. These trajectories provide a comprehensive overview of the energy landscape for Li transport, which is a critical factor in determining the electrochemical performance of the proposed TMCC anode.

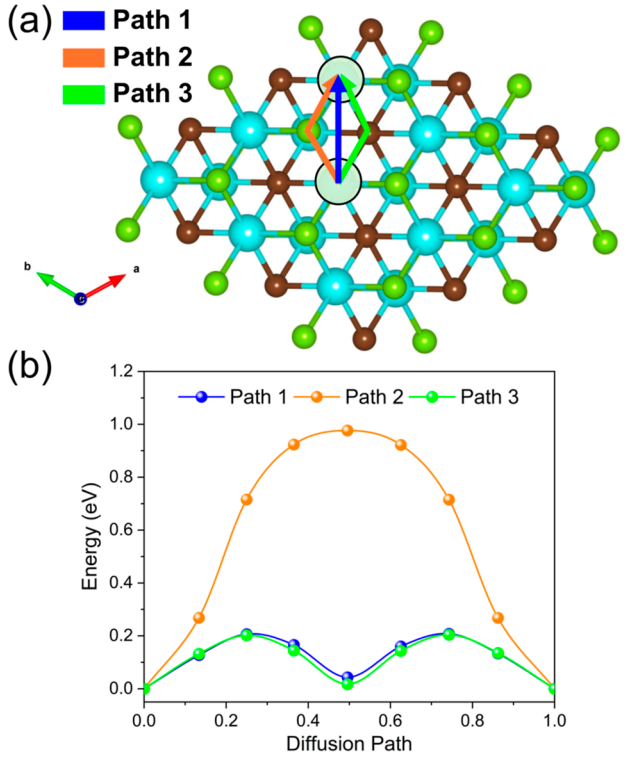

Figure 4. (a) Three studied migration pathways for Li over Zr_2Se_2C monolayer and the (b) associated energy barriers through CI-NEB approach.

The CI-NEB calculations reveal favorable lithium diffusion kinetics along Paths 1 and 3, with energy barriers of 0.209 and 0.205 eV, respectively. In contrast, Path 2 exhibits a significantly higher diffusion barrier of 0.918 eV. This elevated value can be attributed to the presence of selenium atoms, which are located at the outermost layer of the Zr_2Se_2C monolayer. As the Li atom moves across Se sites, enhanced charge transfer interactions are expected, thereby increasing the energy required for migration along this path. Moreover, the Zr site, identified as the most thermodynamically stable adsorption position, likely facilitates stronger charge exchange with neighboring Se atoms. This observation aligns with the increased energy barrier encountered in Path 2, confirming a direct correlation between local bonding environments and ion mobility.

The low diffusion barriers calculated for Paths 1 and 3 underscore the excellent ion transport properties of Zr_2Se_2C, positioning it as a highly promising TMCC-based anode material. These values are comparable to those of similar compounds, such as Nb_2S_2C (0.23 eV) and Nb_2Se_2C (0.20 eV). Furthermore, Zr_2Se_2C outperforms several well-known 2D materials, including borophene (0.60 eV),[41] HOP-graphene (0.70 eV),[42] and $Ti_3C_2O_2$ MXene (0.42 eV).[43]

Li Storage Properties. Building on the single-atom adsorption analysis (see previous section), the lithiation mechanism of the Zr_2Se_2C monolayer is further explored using a double-sided adsorption approach. In this configuration, Li atoms are symmetrically introduced above and below the substrate to maximize capacity while preserving structural integrity. The lithiation process begins with the adsorption of a single lithium layer, targeting the top sites above Zr atoms, which were previously identified as the most energetically favorable adsorption positions. To minimize structural perturbations and better understand the progressive lithiation behavior, Li atoms are incrementally added in a stepwise manner, as illustrated in Figure 5. In this initial stage, a total of 18 Li atoms are uniformly adsorbed across the Zr_2Se_2C TMCC surface. The shortest computed Li−Se distance in this fully occupied configuration is 2.44 Å. Notably, this value is slightly smaller than the 2.51 Å observed in the single-atom adsorption case, indicating that the introduction of a complete Li layer does not significantly disturb the host structure or induce unfavorable interactions. These findings

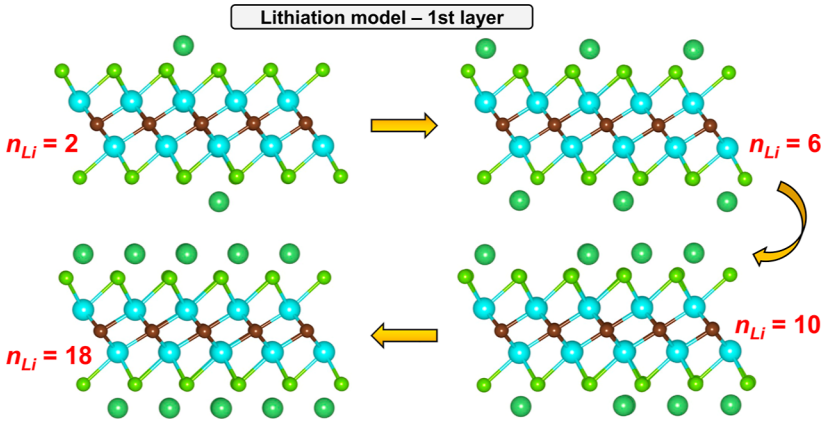

Figure 5. Lithiation scheme for a double-sided Li adsorption (1st layer) on 2D Zr_2Se_2C material.

https://doi.org/10.1021/acsanm.5c03369
ACS Appl. Nano Mater. 2025, 8, 20792−20800

suggest that Zr_2Se_2C maintains structural stability even under increased Li loading, highlighting its potential as a robust candidate for high-capacity anode applications.

The theoretical lithium storage capacity of the 2D Zr_2Se_2C can be estimated using the following expression[44,45]

$$C_Q = \frac{nzF}{W} \times 1000 \quad (3)$$

where n is the number of adsorbed Li atoms, z is the valency of lithium (equal to 1), F is the Faraday constant (26.801 Ah/mol), and W is the molecular weight of the pristine Zr_2Se_2C substrate. Using this relation, a theoretical capacity of 152 mAh/g is obtained for a single Li layer symmetrically adsorbed on both sides of the monolayer. This capacity is comparable to experimentally reported values for related MXene-based materials, such as Ti_2CO_2 (110 mAh/g) and Nb_2CO_2 (170 mAh/g).[19] However, to enhance the energy storage performance of 2D materials, multilayer lithiation strategies have been extensively investigated in both experimental and computational studies.[46−49] Inspired by these findings, we systematically explore the electrochemical storage behavior of 2D Zr_2Se_2C under increasing Li coverage, aiming to assess its full theoretical capacity and multilayer lithiation potential.

To further investigate the multilayer lithiation behavior, single-atom adsorption analysis was repeated to identify the most energetically favorable binding sites for Li atoms in the second and third adsorption layers. Our results indicate that lithium preferentially occupies sites following a Zr−Se−C vertical alignment, corresponding to the first, second, and third Li layers, respectively. The fully lithiated configuration of the Zr_2Se_2C monolayer, containing a total of 54 adsorbed Li atoms, is illustrated in Figure 6a. The interlayer distances

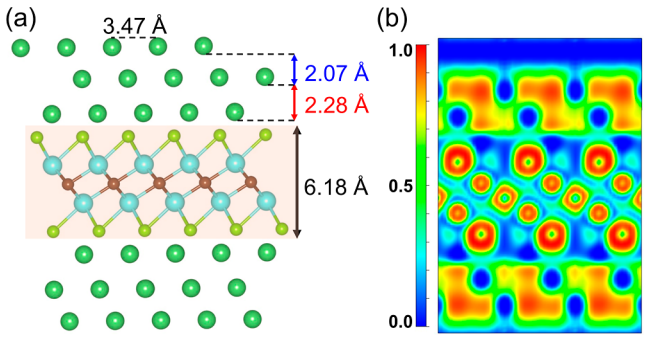

Figure 6. (a) Result of multilayer approach (3-Li layers) over 2D Zr_2Se_2C structure and its (b) electron localization function (ELF) map.

between successive Li layers were found to be 2.28 Å (first to second layer) and 2.07 Å (second to third layer), both of which are noticeably larger than the 1.40 Å spacing observed between the first Li layer and the Se surface atoms. This trend suggests that the interaction strength between Li atoms weakens with increasing coverage, likely due to repulsive Li−Li interactions.

To gain deeper insights into the nature of bonding and charge distribution, the electron localization function (ELF) of the fully lithiated structure is shown in Figure 6b. In the ELF map, red regions represent strong electron localization (ELF ≈ 1.0), while blue regions correspond to low electron density (ELF ≈ 0.0). The Li−Se interaction exhibits low ELF values (ELF < 0.5), confirming its ionic character and supporting the high charge transfer observed in the first layer. Conversely, the interaction between Li atoms is characterized by very low electron localization and is dominated by electrostatic repulsion, which accounts for the increased spacing between Li layers in the higher coverage regime.

The evolution of the adsorption energy with increasing lithium coverage on the Zr_2Se_2C TMCC monolayer was evaluated and is presented in Figure 7a. As additional Li atoms are introduced, the adsorption energy gradually decreases from −2.86 eV to −1.67 eV. This trend reflects a progressive stabilization of the system as charge from Li is evenly distributed across the substrate, leading to a lower overall energy configuration. Notably, the drop in E_{ads} becomes less pronounced between the second and third Li layers, indicating a saturation point in the adsorption process and suggesting that the system approaches a thermodynamically stable state at higher coverage. The corresponding theoretical capacities for single, double, and triple Li-layer configurations are calculated to be 152, 304, and 456 mAh/g, respectively, as illustrated in Figure 7b. These values position Zr_2Se_2C among the most promising TMCC-based anode materials, with substantial energy storage performance.

To gain enhanced insight into the electronic effects of progressive lithiation on the Zr_2Se_2C monolayer, detailed electronic structure calculations were performed through PDOS plots (see Figure S1). At the first Li adsorption layer (Figure S1a), a pronounced hybridization between Li and Zr states is observed, particularly around 0.5 eV above the Fermi level, indicating strong interaction. As additional Li layers are deposited onto the Zr_2Se_2C substrate, significant hybridization emerges within both the valence and conduction bands. Notably, pronounced peaks corresponding to orbital interactions between Li and Zr atoms appear near −0.9, 0.8, and 2.2 eV. These features reflect substantial electronic coupling between the adsorbed Li atoms and the TMCC host lattice. Furthermore, PDOS analysis confirms that the metallic character of Zr_2Se_2C is preserved throughout the lithiation process, a crucial attribute for maintaining efficient electron transport in anodic applications.

The thermal stability of the proposed multilayer lithium storage configuration on the 2D Zr_2Se_2C electrode was further evaluated using ab initio molecular dynamics (AIMD) simulations at room temperature (see Figure 8). The energy profile over the 5 ps simulation exhibits a smooth and stable behavior, confirming the reliability of the system under thermal fluctuations. Moreover, the final AIMD snapshot demonstrates that the Zr_2Se_2C monolayer can effectively accommodate a high density of Li atoms without significant structural distortion. Notably, pronounced Li-ion mobility is observed between the layers, yet no aggregation or clustering of Li atoms occurs. At the end of the AIMD simulation, we observed a 3.48% expansion in the layer thickness. Additionally, the average in-plane Li−Li bond length decreased slightly from 3.45 Å to 3.36 Å, confirming that multilayer stacking does not induce significant lattice distortions under thermal perturbation. This behavior suggests that the material can facilitate facile lithium insertion and extraction, highlighting its promising potential for efficient charge/discharge cycling in TMCC-based battery applications.

The open-circuit voltage (OCV) profile was calculated to evaluate the electrochemical stability and safety of the Zr_2Se_2C anode. The OCV values were estimated using the average

https://doi.org/10.1021/acsanm.5c03369
ACS Appl. Nano Mater. 2025, 8, 20792−20800

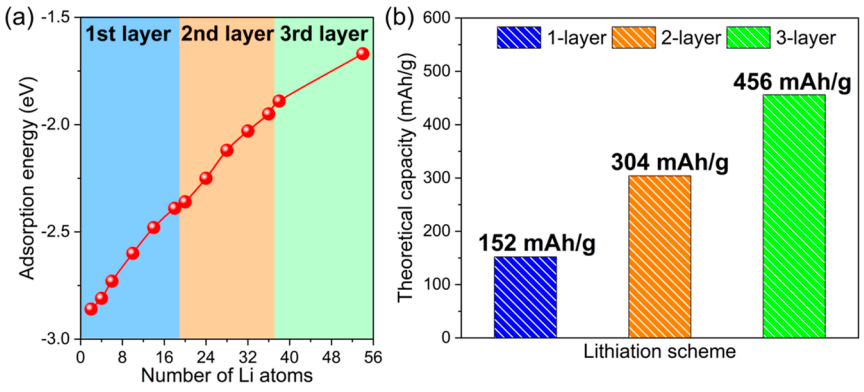

Figure 7. (a) Adsorption energy results for lithiation on Zr_2Se_2C monolayer. (b) Theoretical capacities depicted for each Li storage approach (1-layer, 2-layer, and 3-layer).

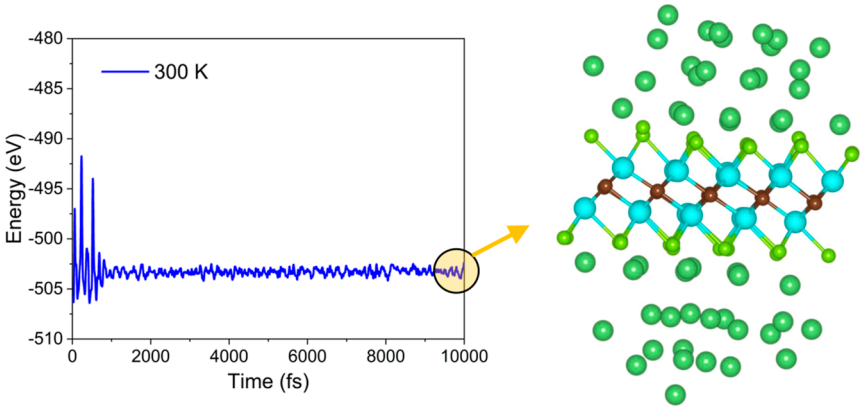

Figure 8. Energy fluctuation and final snapshot of ab initio molecular dynamics (AIMD) for 3-Li layers scheme over Zr_2Se_2C TMCC.

adsorption energies of lithium atoms according to the relation[44,50]

$$\mathrm{OCV} = \frac{-(E_{Zr_2Se_2C+xLi} - E_{Zr_2Se_2C} - xE_{Li})}{xze} \quad (4)$$

where x denotes the number of adsorbed Li atoms and e is the elementary charge. Negative average adsorption energies correspond to thermodynamically favorable adsorption, which translates into positive OCV values, indicating stable and safe electrode operation.

Figure 9a illustrates the OCV profile as a function of lithium concentration on the Zr_2Se_2C anode. The voltage decreases progressively with increasing Li content, as expected. At the lowest Li coverage, the OCV reaches 1.90 V, dropping to 0.17 V for a fully occupied first Li layer (18 Li atoms). Subsequent adsorption of additional Li layers maintains positive OCV values of 0.07 and 0.04 V for the bilayer and trilayer configurations, respectively. The presence of a plateau during the second lithiation step further supports the electrochemical stability of the multilayer Li storage on 2D Zr_2Se_2C. An average OCV of approximately 0.53 V confirms that this material offers a promising anodic performance suitable for lithium-ion battery applications. The obtained results for 2D Zr_2Se_2C are close to the voltage window required for practical applications, where low but positive values are essential to ensure a safe lithiation mechanism.[51]

The structural stability of lithiation on an electrode can be theoretically assessed by computing the formation energy ($E_f(x)$) for different Li concentrations (x). Here, as the number of Li atoms increases on the TMCC monolayer, the formation energy of the material with intermediate lithium content is expressed following[52,53]

$$E_{f(x)} = E_{(Li_xZr_2Se_2C)} - xE_{(Li)} - (1-x)E_{(Zr_2Se_2C)} \quad (5)$$

where E is the total energy. In eq 5, the reference states are defined considering different lithiation steps, i.e., x = 0, 0.04, 0.4, 0.62, 0.8, and 1.2. As shown in Figure 9b, all lithiated compounds of 2D Zr_2Se_2C lie on the convex hull. This parameter indicates the thermodynamic feasibility of the proposed anode material.

In Table 1, we compare the main theoretical parameters of 2D Zr_2Se_2C with those reported for other 2D anode materials. The results highlight its superior theoretical capacity compared to its analogues, i.e., Nb_2S_2C (194 mAh/g),[22] Ta_2Se_2C (404 mAh/g),[24] and Ta_2S_2C (367 mAh/g).[54] As expected, bare MXenes such as Ti_3C_2[55] and V_4C_3[56] present smaller diffusion energy barriers (0.07 and 0.05 eV, respectively) than 2D Zr_2Se_2C (0.20 eV), since the binding strength of metals over these substrates is weaker than the metal−S or metal−Se interactions in 2D TMCCs. Also regarding diffusion kinetics, 2D Zr_2Se_2C also exhibits competitive performance relative to these 2D TMCCs and to carbon allotropes such as HOP-graphene,[42] Me-graphene,[57] CYC-CTF0,[58] CTF0,[59] and Athos-graphene.[60] A similar trend is observed for the average OCV profile. Overall, the proposed 2D Zr_2Se_2C is verified as a viable alternative anode material due to its competitive electrochemical performance evidenced by computational simulations.

https://doi.org/10.1021/acsanm.5c03369
ACS Appl. Nano Mater. 2025, 8, 20792−20800

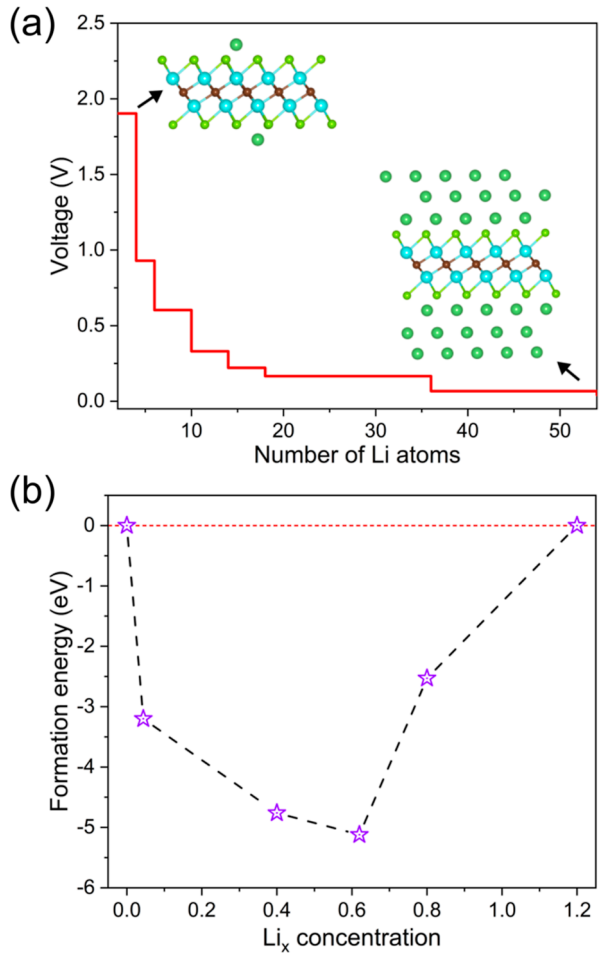

Figure 9. (a) Open-circuit voltage (OCV) profile and (b) formation energy convex hull plot for Li storage on Zr_2Se_2C monolayer.

Table 1. Performance Comparison of the Li Storage Capacity, Energy Barrier and Average OCV Calculated for 2D Zr_2Se_2C and Those Reported Theoretically for 2D Anode-Based Materials

System	Capacity (mAh/g)	Energy barrier (eV)	Average OCV (V)
Zr_2Se_2C (this work)	456	0.20	0.53
Nb_2S_2C[22]	194	0.23	0.92
Ta_2Se_2C[24]	404	0.26	0.34
Ta_2S_2C[54]	367	0.21	0.57
Ti_3C_2[55]	448	0.07	0.43
V_4C_3[56]	223	0.05	0.38
HOP-graphene[42]	1338	0.70	0.42
Me-graphene[57]	613	0.48	-
CYC-CTF0[58]	585	0.17	1.10
CTF0[59]	462	0.07	-
Athos-graphene[60]	837	0.30	0.54

CONCLUSIONS

Motivated by ongoing advances in the synthesis and study of two-dimensional (2D) transition metal carbo-chalcogenides (TMCCs), this work investigates the anodic potential of a novel Zr_2Se_2C monolayer using density functional theory (DFT) simulations. Our results demonstrate both the thermal and dynamical stability of 2D Zr_2Se_2C, confirmed through ab initio molecular dynamics (AIMD) simulations and phonon dispersion analyses, respectively. Single-atom lithium adsorption reveals a strong binding affinity accompanied by a significant charge transfer of 0.23 *e*. The lithium diffusion mechanism across the Zr_2Se_2C surface was probed using the climbing image nudged elastic band (CI-NEB) method, yielding a low energy barrier of 0.20 eV, indicative of favorable Li mobility.

Furthermore, both single- and multilayer lithium storage scenarios were examined, with theoretical capacities calculated as 152, 304, and 456 mAh/g for one, two, and three Li layers, respectively. AIMD simulations corroborate the thermal stability of the fully lithiated multilayer configuration. Finally, the open-circuit voltage (OCV) profile for Li adsorption on Zr_2Se_2C spans a favorable range from 1.90 to 0.04 V, with an average value of 0.53 V, supporting its promise as an efficient anode material for lithium-ion batteries.

ASSOCIATED CONTENT

Data Availability Statement

Data supporting the results can be accessed by contacting the corresponding author.

Supporting Information

The Supporting Information is available free of charge at https://pubs.acs.org/doi/10.1021/acsanm.5c03369.

The lattice parameters of 2D Zr_2Se_2C and other 2D TMCCs (Ta_2Se_2C, Nb_2Se_2C, Ta_2S_2C, and Nb_2S_2C), as well as the calculated elastic constants for each of these structures, are presented. Additionally, total density of states (DOS) plots for the lithiation steps are provided (PDF)

AUTHOR INFORMATION

Corresponding Authors

Nicolas F. Martins − *Modeling and Molecular Simulation Group, São Paulo State University (UNESP) School of Sciences, Bauru 17033-360 São Paulo, Brazil;* orcid.org/0000-0001-7653-0428; Email: nicolas.ferreira@unesp.br

Julio R. Sambrano − *Modeling and Molecular Simulation Group, São Paulo State University (UNESP) School of Sciences, Bauru 17033-360 São Paulo, Brazil;* Email: jr.sambrano@unesp.br

Authors

Fredy Mamani Gonzalo − *Modeling and Molecular Simulation Group, São Paulo State University (UNESP) School of Sciences, Bauru 17033-360 São Paulo, Brazil*

José A. S. Laranjeira − *Modeling and Molecular Simulation Group, São Paulo State University (UNESP) School of Sciences, Bauru 17033-360 São Paulo, Brazil;* orcid.org/0000-0002-8366-7227

Victor J. R. Rivera − *Modeling and Molecular Simulation Group, São Paulo State University (UNESP) School of Sciences, Bauru 17033-360 São Paulo, Brazil*

Pablo A. Denis − *Computational Nanotechnology, DETEMA, Facultad de Química, UDELAR, 11800 Montevideo, Uruguay;* orcid.org/0000-0003-3739-5061

Complete contact information is available at: https://pubs.acs.org/10.1021/acsanm.5c03369

Funding

The Article Processing Charge for the publication of this research was funded by the Coordenacao de Aperfeicoamento

de Pessoal de Nivel Superior (CAPES), Brazil (ROR identifier: 00x0ma614).

Notes

The authors declare no competing financial interest.

■ ACKNOWLEDGMENTS

This work was supported by the Brazilian funding agencies Fundação de Amparo à Pesquisa do Estado de São Paulo—FAPESP (2022/16509-9, 2024/05087-1, 2024/22897-7, and 2024/22899-0) and the National Council for Scientific and Technological Development—CNPq (grant no. 307213/2021-8).

■ REFERENCES

(1) Kim, T.-H.; Park, J.-S.; Chang, S. K.; Choi, S.; Ryu, J. H.; Song, H.-K. The current move of lithium ion batteries towards the next phase. *Adv. Energy Mater.* **2012**, *2*, 860−872.
(2) Nishi, Y. Lithium ion secondary batteries; past 10 years and the future. *J. Power Sources* **2001**, *100*, 101−106.
(3) Yi, R.; Mao, Y.; Shen, Y.; Chen, L. Self-assembled monolayers for batteries. *J. Am. Chem. Soc.* **2021**, *143*, 12897−12912.
(4) Omar, N.; Daowd, M.; Bossche, P. v. d.; Hegazy, O.; Smekens, J.; Coosemans, T.; Mierlo, J. v. Rechargeable energy storage systems for plug-in hybrid electric vehicles—Assessment of electrical characteristics. *Energies* **2012**, *5*, 2952−2988.
(5) Goodenough, J. B.; Kim, Y. Challenges for rechargeable batteries. *J. Power Sources* **2011**, *196*, 6688−6694.
(6) Yoshino, A. The birth of the lithium-ion battery. *Angew. Chem., Int. Ed.* **2012**, *51*, 5798−5800.
(7) Augustyn, V.; Gogotsi, Y. 2D materials with nanoconfined fluids for electrochemical energy storage. *Joule* **2017**, *1*, 443−452.
(8) Ranjan, P.; Gaur, S.; Yadav, H.; Urgunde, A. B.; Singh, V.; Patel, A.; Vishwakarma, K.; Kalirawana, D.; Gupta, R.; Kumar, P. 2D materials: increscent quantum flatland with immense potential for applications. *Nano Convergence* **2022**, *9*, 26.
(9) Mendoza-Sánchez, B.; Gogotsi, Y. Synthesis of two-dimensional materials for capacitive energy storage. *Adv. Mater.* **2016**, *28*, 6104−6135.
(10) Feng, C.; Ma, J.; Li, H.; Zeng, R.; Guo, Z.; Liu, H. Synthesis of molybdenum disulfide (MoS2) for lithium ion battery applications. *Mater. Res. Bull.* **2009**, *44*, 1811−1815.
(11) Bhandavat, R.; David, L.; Singh, G. Synthesis of surface-functionalized WS2 nanosheets and performance as Li-ion battery anodes. *J. Phys. Chem. Lett.* **2012**, *3*, 1523−1530.
(12) Wang, H.; Wang, X.; Wang, L.; Wang, J.; Jiang, D.; Li, G.; Zhang, Y.; Zhong, H.; Jiang, Y. Phase transition mechanism and electrochemical properties of nanocrystalline MoSe2 as anode materials for the high performance lithium-ion battery. *J. Phys. Chem. C* **2015**, *119*, 10197−10205.
(13) Zhou, P.; Collins, G.; Hens, Z.; Ryan, K. M.; Geaney, H.; Singh, S. Colloidal WSe2 nanocrystals as anodes for lithium-ion batteries. *Nanoscale* **2020**, *12*, 22307−22316.
(14) Naguib, M.; Kurtoglu, M.; Presser, V.; Lu, J.; Niu, J.; Heon, M.; Hultman, L.; Gogotsi, Y.; Barsoum, M. W. *MXenes*; Jenny Stanford Publishing, 2023; pp 15−29.
(15) Zhang, Y.; Ma, C.; He, W.; Zhang, C.; Zhou, L.; Wang, G.; Wei, W. MXene and MXene-based materials for lithium-sulfur batteries. *Prog. Nat. Sci. Mater. Int.* **2021**, *31*, 501−513.
(16) Liu, R.; Cao, W.; Han, D.; Mo, Y.; Zeng, H.; Yang, H.; Li, W. Nitrogen-doped Nb2CTx MXene as anode materials for lithium ion batteries. *J. Alloys Compd.* **2019**, *793*, 505−511.
(17) Liu, F.; Liu, Y.; Zhao, X.; Liu, K.; Yin, H.; Fan, L.-Z. Prelithiated V2C MXene: a high-performance electrode for hybrid magnesium/lithium-ion batteries by ion cointercalation. *Small* **2020**, *16*, 1906076.
(18) Sunkari, D.; Deshmukh, K.; Panda, S.; Pasha, S. K. Recent progress in MXene-based materials for lithium-ion and lithium-sulphur batteries: A comprehensive review. *J. Energy Storage* **2024**, *92*, 112017.
(19) Naguib, M.; Come, J.; Dyatkin, B.; Presser, V.; Taberna, P.-L.; Simon, P.; Barsoum, M. W.; Gogotsi, Y. MXene: a promising transition metal carbide anode for lithium-ion batteries. *Electrochem. Commun.* **2012**, *16*, 61−64.
(20) Pang, X.; Wu, T.; Gu, Y.; Wang, D.; Che, X.; Sun, D.; Huang, F. Nb2Se2C: a new compound as a combination of transition metal dichalcogenide and MXene for oxygen evolution reaction. *Chem. Commun.* **2020**, *56*, 9036−9039.
(21) Majed, A.; Kothakonda, M.; Wang, F.; Tseng, E. N.; Prenger, K.; Zhang, X.; Persson, P. O.; Wei, J.; Sun, J.; Naguib, M. Transition Metal Carbo-Chalcogenide "TMCC:" A New Family of 2D Materials. *Adv. Mater.* **2022**, *34*, 2200574.
(22) Jing, Y.; Liu, J.; Zhou, Z.; Zhang, J.; Li, Y. Metallic Nb2S2C monolayer: a promising two-dimensional anode material for metal-ion batteries. *J. Phys. Chem. C* **2019**, *123*, 26803−26811.
(23) Loni, E.; Majed, A.; Zhang, S.; Thangavelu, H. H.; Dun, C.; Tabassum, A.; Eisawi, K.; Urban, J. J.; Persson, P. O.; Montemore, M. M. Two-Dimensional Tantalum Carbo-Selenide for Hydrogen Evolution. *ACS Nano* **2025**, *19*, 3185−3196.
(24) Martins, N. F.; Laranjeira, J. A.; Aparicio-Huacarpuma, B. D.; Ribeiro Junior, L. A.; Sambrano, J. R. Computational Characterization of the Novel Ta2Se2C Transition Metal Carbo-Chalcogenide as Anode Material for Li and Na-Ion Batteries. *J. Phys. Chem. C* **2025**, *129*, 16559−16568.
(25) Sun, J.; Yu, R.; Legut, D.; Francisco, J. S.; Zhang, R. Rational Design of Highly Stable and Active Single-Atom Modified S-MXene as Cathode Catalysts for Li-S Batteries. *Adv. Mater.* **2025**, *37*, 2501523.
(26) Jethawa, U.; Chaudhari, A.; Chakraborty, B. Unveiling the potential of newly synthesized 2D TMCC monolayer for H2S gas sensing: A DFT study. *Surf. Interfaces* **2024**, *54*, 105098.
(27) Lakshmy, S.; Kalarikkal, N.; Chakraborty, B. Cu-incorporated novel 2D Transition metal carbo chalcogenide Nb2S2C monolayer for Superior Nitrobenzene sensing: A theoretical study. *Surf. Interfaces* **2024**, *47*, 104209.
(28) Upadhyay, S. N.; Singh, J. K. Unraveling the Catalytic Potential of 2D Nb2Se2C for Lithium Polysulfide Conversion: A DFT Study. *ACS Appl. Energy Mater.* **2025**, *8*, 6733−6745.
(29) Hu, T.; Wang, M.; Cai, C.; Cheng, R.; Wang, J.; Guo, C.; Ren, L.; Li, C. M.; Wang, X. Van der Waals Transition Metal Carbo-Chalcogenides: Theoretical Screening and Charge Storage. *Small* **2024**, *20*, 2402076.
(30) Herabad, S. R.; Soleimani, H. R.; Mohebpour, M. A. Novel 2D Transition Metal Carbo-Chalcogenides as Anode Materials: A Comparative Study of Sc2S2C and Sc2Se2C Monolayers. *J. Phys. Chem. Solids* **2025**, *205*, 112779.
(31) Kresse, G.; Joubert, D. From ultrasoft pseudopotentials to the projector augmented-wave method. *Phys. Rev. B: Condens. Matter Mater. Phys.* **1999**, *59*, 1758.
(32) Perdew, J. P.; Burke, K.; Ernzerhof, M. Generalized Gradient Approximation Made Simple. *Phys. Rev. Lett.* **1996**, *77*, 3865−3868.
(33) Blöchl, P. E. Projector augmented-wave method. *Phys. Rev. B: Condens. Matter Mater. Phys.* **1994**, *50*, 17953−17979.
(34) Grimme, S.; Antony, J.; Ehrlich, S.; Krieg, H. A consistent and accurate ab initio parametrization of density functional dispersion correction (DFT-D) for the 94 elements H-Pu. *J. Chem. Phys.* **2010**, *132*, 154104.
(35) Tadano, T.; Tsuneyuki, S. Self-consistent phonon calculations of lattice dynamical properties in cubic SrTiO3 with first-principles anharmonic force constants. *Phys. Rev. B: Condens. Matter Mater. Phys.* **2015**, *92*, 054301.
(36) Tadano, T.; Gohda, Y.; Tsuneyuki, S. Anharmonic force constants extracted from first-principles molecular dynamics: applications to heat transfer simulations. *J. Phys.: Condens. Matter* **2014**, *26*, 225402.
(37) Hoover, W. G. Canonical dynamics: Equilibrium phase-space distributions. *Phys. Rev. A* **1985**, *31*, 1695.

https://doi.org/10.1021/acsanm.5c03369
ACS Appl. Nano Mater. 2025, 8, 20792−20800

(38) Mouhat, F.; Coudert, F.-X. Necessary and sufficient elastic stability conditions in various crystal systems. *Phys. Rev. B: Condens. Matter Mater. Phys.* **2014**, *90*, 224104.
(39) Wang, Y.; Wang, S.; Zhang, Y.; Song, N.; Luo, S.; Xu, B.; Wang, F. Two-dimensional Zr2C monolayer as anode material for Li, Na and K ion batteries. *Chem. Phys.* **2025**, *589*, 112521.
(40) Li, H.; Xie, Z.; Gao, T.; Liu, J.; Lu, W.; Liu, Y.; Wang, S. Role of Oxygen and Halogen Functionalization in Tuning the Surface Properties of Zr3C2T2MXene for Lithium Storage: A Density Functional Theory Study. *Materials* **2025**, *18*, 1237.
(41) Zhang, X.; Hu, J.; Cheng, Y.; Yang, H. Y.; Yao, Y.; Yang, S. A. Borophene as an extremely high capacity electrode material for Li-ion and Na-ion batteries. *Nanoscale* **2016**, *8*, 15340−15347.
(42) Martins, N. F.; Laranjeira, J. A.; Lima, K. A.; Cabral, L. A.; Ribeiro, L. A., Junior; Sambrano, J. R. HOP-graphene: A high-capacity anode for Li/Na-ion batteries unveiled by first-principles calculations. *Appl. Surf. Sci.* **2025**, *710*, 163737.
(43) Yuan, K.; Hao, P.; Hu, X.; Zhang, J.; Zhou, Y. Experimental and computational studies on S-decorated Ti3C2MXene as anode material in Li-ion batteries. *J. Mater. Sci.* **2022**, *57*, 7001−7011.
(44) Patel, P.; Patel, S.; Chodvadiya, D.; Dalsaniya, M. H.; Kurzydłowski, D.; Jha, P. K. Two-dimensional α-SiX (X= N, P) monolayers as efficient anode material for Li-ion batteries: A first-principles study. *ACS Appl. Nano Mater.* **2023**, *6*, 2103−2115.
(45) Haouam, M.; Abdullahi, Y. Z.; Zanat, K.; Ersan, F. Boron phosphide (BP) biphenylene and graphenylene networks as anode and anchoring materials for Li/Na-ion and Li/Na−S batteries. *Appl. Surf. Sci.* **2024**, *662*, 160096.
(46) Kim, S. J.; Naguib, M.; Zhao, M.; Zhang, C.; Jung, H.-T.; Barsoum, M. W.; Gogotsi, Y. High mass loading, binder-free MXene anodes for high areal capacity Li-ion batteries. *Electrochim. Acta* **2015**, *163*, 246−251.
(47) Mashtalir, O.; Lukatskaya, M. R.; Zhao, M.-Q.; Barsoum, M. W.; Gogotsi, Y. *MXenes*; Jenny Stanford Publishing, 2023; pp 401−414.
(48) Patel, P.; Patel, S.; Chodvadiya, D.; Dalsaniya, M. H.; Kurzydłowski, D.; Kurzydłowski, K. J.; Jha, P. K. A density functional theory study on the assessment of α-CN and α-CP monolayers as anode material in Li-ion batteries. *J. Energy Storage* **2023**, *71*, 108074.
(49) Luo, J.; Zheng, J.; Nai, J.; Jin, C.; Yuan, H.; Sheng, O.; Liu, Y.; Fang, R.; Zhang, W.; Huang, H.; et al. Atomic Sulfur Covalently Engineered Interlayers of Ti_3C_2 MXene for Ultra-Fast Sodium-Ion Storage by Enhanced Pseudocapacitance. *Adv. Funct. Mater.* **2019**, *29*, 1808107.
(50) Martins, N. F.; Laranjeira, J. A.; Fabris, G. S.; Denis, P. A.; Sambrano, J. R. Irida-graphene as a high-performance anode for sodium batteries. *J. Energy Storage* **2024**, *104*, 114637.
(51) Wang, Y.; Zhou, M.; Xu, L.-C.; Zhao, W.; Li, R.; Yang, Z.; Liu, R.; Li, X. Achieving superior high-capacity batteries with the lightest Ti2C MXene anode by first-principles calculations: Overarching role of S-functionate (Ti 2CS2) and multivalent cations carrier. *J. Power Sources* **2020**, *451*, 227791.
(52) Van der Ven, A.; Aydinol, M. K.; Ceder, G.; Kresse, G.; Hafner, J. First-principles investigation of phase stability in Li_xCoO_2. *Phys. Rev. B: Condens. Matter Mater. Phys.* **1998**, *58*, 2975−2987.
(53) Gonzalo, F. M.; Laranjeira, J. A.; Rivera, V. J.; Martins, N. F.; Sambrano, J. R.; Piotrowski, M. J.; Flores, E. M. Enhanced lithium storage in the novel ZrNbCO2 Janus MXene. *Surf. Interfaces* **2025**, *73*, 107541.
(54) Wu, M.; Xin, B.; Yang, W.; Li, B.; Dong, H.; Cheng, Y.; Wang, W.; Lu, F.; Wang, W.-H.; Liu, H. Metallic monolayer Ta2CS2: an anode candidate for Li+, Na+, K+, and Ca2+ ion batteries. *ACS Appl. Energy Mater.* **2020**, *3*, 10695−10701.
(55) Er, D.; Li, J.; Naguib, M.; Gogotsi, Y.; Shenoy, V. B. Ti3C2MXene as a high capacity electrode material for metal (Li, Na, K, Ca) ion batteries. *ACS Appl. Mater. Interfaces* **2014**, *6*, 11173−11179.
(56) Peng, Q.; Rehman, J.; Eid, K.; Alofi, A. S.; Laref, A.; Albaqami, M. D.; Alotabi, R. G.; Shibl, M. F. Vanadium carbide (V4C3) MXene as an efficient anode for Li-ion and Na-ion batteries. *Nanomaterials* **2022**, *12*, 2825.
(57) Zhao, W.-H.; Li, F.-Y.; Zhang, H.-X.; Eglitis, R. I.; Wang, J.; Jia, R. Doping at sp3-site in Me-graphene (C568) for new anodes in rechargeable Li-ion battery. *Appl. Surf. Sci.* **2023**, *607*, 154895.
(58) Kaviani, S.; Piyanzina, I.; Tayurskii, D. A.; Nedopekin, O. V. A DFT modeling of 4-cyclohexene-1,3-dione embedded in covalent triazine framework as a stable anode material for Li-ion batteries. *Mater. Chem. Phys.* **2024**, *322*, 129592.
(59) Kaviani, S.; Shamsieva, A.; Piyanzina, I.; Tayurskii, D. A.; Nedopekin, O. V. Enhanced anodic performance of CTF0 monolayer for Li-ion batteries through F and Si co-doping: A DFT insight. *Colloids Surf., A* **2025**, *705*, 135752.
(60) Lima, K. A.; Laranjeira, J. A.; Martins, N. F.; Sambrano, J. R.; Dias, A. C.; Galvão, D. S.; Junior, L. A. R. Athos-Graphene: Computational discovery of an art-inspired 2D carbon anode for lithium-ion batteries. *J. Energy Storage* **2025**, *133*, 117868.

https://doi.org/10.1021/acsanm.5c03369
ACS Appl. Nano Mater. 2025, 8, 20792−20800